e-ISSN: 2149-4584

Erzincan University Journal of Science and Technology

EJSAT 2025, 18 (3) 763-780

Research Article

Calculation of Different Intensity Ratios of Samples with Atomic Numbers Between 9≤Z≤83 Using the Dilution Technique

Tuba Akkuş[1], Mehmet Fatih Temiz[2]

[1]Department of Physics, Faculty of Arts and Sciences, Erzincan Binali Yıldırım University, Erzincan, Türkiye, 24100.
[2]Department of Physics, Graduate School of Natural and Applied Sciences, Erzincan Binali Yıldırım University, Erzincan, Türkiye, 24100.

Received: 12/02/2025 **Revised:** 21/06/2025 **Accepted:** 30/06/2025, **Published:** 31/12/2025

Abstract

In this study, the variation of different intensity ratios with the mean atomic number was investigated in the Energy Dispersive X-ray Fluorescence system for qualitative analysis. Fourteen different samples were used in the study. The average atomic numbers of the samples obtained by diluting with cellulose are between 9.74 and 83.00. The samples were excited by photons with 59.54 kiloelectron volt energy from the Americium-241 source and an HpGe detector with 182 electron volt resolution at 5.9 kiloelectron volt was used. The obtained results show that different scattering intensity ratios can be used with high reliability for complex materials in qualitative analysis. In this study, different intensity ratios were plotted as a function of the average atomic number and best fit curves were created. From the obtained fit curves, it was seen that the intensity ratios $I_{L_\alpha}/I_{sc_{(L_\alpha)}}$, $I_{L_\beta}/I_{sc_{(L_\beta)}}$ $I_{K_{\alpha_2}}/I_{sc_{(K_{\alpha_2})}}$ and $I_{K_{\alpha_1}}/I_{sc_{(K_{\alpha_1})}}$ were the best spectral ratio methods that can be used to determine the effective atomic number.

Keywords: EDXRF, intensity ratio, mean atomic number, qualitative analysis.

Seyreltme Tekniği Kullanılarak Atom Numarası 9≤Z≤83 Arasında Olan Numunelerin Farklı Şiddet Oranlarının Hesaplanması

Öz

Bu çalışmada, kalitatif analiz için Enerji Dağılımlı X-ışını Floresan sisteminde farklı şiddet oranlarının ortalama atom numarasına göre değişimi araştırılmıştır. Araştırmada 14 farklı numune kullanıldı. Selüloz ile seyreltilerek elde edilen numunelerin ortalama atom numaraları 9,74 ile 83,00 arasındadır. Numuneler, Americium-241 kaynağından gelen 59,54 kiloelektron volt enerjili fotonlarla uyarıldı ve 5,9 kiloelektron voltta 182 elektron volt çözünürlüğe sahip bir HpGe dedektörü kullanıldı. Elde edilen sonuçlar, kalitatif analizde karmaşık malzemeler için farklı saçılma şiddet oranlarının yüksek güvenilirlikle kullanılabileceğini göstermektedir. Bu çalışmada farklı şiddet oranları, ortalama atom numarasının fonksiyonu olarak çizildi ve en uygun fit eğrileri oluşturuldu. Elde edilen fit eğrilerinden $I_{L_\alpha}/I_{sc_{(L_\alpha)}}$, $I_{L_\beta}/I_{sc_{(L_\beta)}}$ $I_{K_{\alpha_2}}/I_{sc_{(K_{\alpha_2})}}$ ve $I_{K_{\alpha_1}}/I_{sc_{(K_{\alpha_1})}}$ şiddet oranlarının etkin atom numarasının belirlenmesinde kullanılabilecek en iyi spektral oran yöntemleri olduğu görüldü.

Anahtar Kelimeler: EDXRF, şiddet oranı, ortalama atom numarası, kalitatif analiz.

Corresponding Author: takkus@erzincan.edu.tr

Cite this Article: Erzincan University Journal of Science and Technology 2025, 18(3) 763-780. https://doi.org/10.18185/erzifbed.1638042

1. Introduction

Each material has a specific color, texture and appearance. However, these features are insufficient to describe this material. To determine beyond doubt the exact composition of a material, physical and chemical properties generally need to be evaluated. Melting point, color, boiling point, density, electrical conductivity, thermal conductivity, refractive index, and coefficient of expansion are some of the more common physical properties measured to identify an unknown substance. Many of these properties are measurable values that can be compared to known values of elements and compounds. More detailed physical tests deal with measurements based on the internal structure of a material. Depending on the arrangement of particles within a substance, they interact with electromagnetic radiation in different ways. The result of these interactions is an electromagnetic spectrum, which is a pictorial representation of the absorption and emission of electromagnetic radiations of varying energy as they strike and pass through a substance.

Qualitative analysis is a method that examines which elements or compounds a substance consists of and covers a series of analytical chemistry techniques that measure properties that provide non-numerical information about the sample, such as color change, gas release, precipitate formation or dissolution, and whether it has radioactive properties. Quantitative analysis, on the other hand, gives numerical information about the presence rates of the components of a sample, in other words, their relative amounts. There are many areas where qualitative and quantitative analysis is used. In the research of anti-cancer drugs in medicine [1], in the investigation of skin flora from a bacterial perspective [2] ,in the investigation of factors affecting oil production [3], in the analysis of elements in cataracts [4] in determining benign and malignant tumors [5], in researching the contents of ores [6] in determining the structural properties of multi-component bioglasses [7], in investigating selenium species in mushrooms [8], in determining the active ingredients of drugs [9], in detecting fracture patterns of ceramics [10], in thrombin analysis in serum [11], in evaluating air quality [12], in determining the components of hydrocarbon mixtures [13], in the determination of monomers in polyester in food contact materials [14], in the type and quantity analysis of polyphenols in plants [15] ,in the analysis of spectral properties in multicomponent liquid mixtures [16], in measuring the microstructural properties of bones and in determining the degree of mineralization of bones [17], in investigating the dynamics of some diseases [18], in supporting the analytical results of the model applied in biomedical interventions [19], in the determination of clusters in water solutions of alcohols [20], in crystallographic analysis in electroceramics. in evaluating tissues [21], in determining calibration methods in analytical chemistry and in identification analyzes of uncontrolled analytical effects [22], in investigating the nutritional benefits and risks that may occur with the consumption of mussels [23], in sintering analyzes of metals in manufacturing applications [24],in the surface analysis of orthodontic brackets [25] in the analysis of colorants found in candies [26]. There are many studies in the literature about different intensity ratios. Some researchers have studied K x-ray intensity ratios. Kβ/Kα intensity ratios of some copper and zinc alloys were examined at 22.69 keV [27]. Kα/Kβ intensity ratios have been calculated experimentally for elements with atomic numbers in the range of $28 \leq Z \leq 39$. The results obtained were compared with theoretical values [28]. K x-ray intensity ratios of some heavy elements

experimentally calculated using a HPGe detector in the EDXRF system [29]. Kβ/Kα x-ray intensity ratios of Cr, Mn, Fe and Co elements were determined experimentally at 8.735 keV energy [30]. The changes in the Kβ/Kα intensity ratios of MoCu alloys at different concentrations in the external magnetic field were examined [31]. The valence electronic structure of Ni in Ni-B alloy coatings was determined using the Kβ/Kα x-ray intensity ratio [32]. The Kβ/Kα intensity ratios of 3d and 4d transition metals were examined in the external magnetic field [33].

Some researchers have also studied L x-ray intensity ratios. L x-ray intensity ratios of some heavy elements at 20.48 keV were calculated [34]. L x-ray intensity ratios of Hg, Pb and Bi compounds calculated at 59.54 keV [35]. L x-ray intensity ratios of elements with atomic number 74≤Z≤92 calculated at 31.635 keV energy [36]. L x-ray intensity ratios of Dy, Ho, Yb, W, Hg, Tl and Pb elements investigated at 59.54 keV [37]. Different L x-ray intensity ratios have been calculated for Dy, Ho and Er elements and some compounds of these elements [38].Investigated the change of L x-ray intensity ratios with temperature [39].

In this study, total scattering intensity ratios were calculated at four different energies and $(I_{coh} + I_{Comp})/(\mu/\rho)_{L_\alpha}$, $(I_{coh} + I_{Comp})/(\mu/\rho)_{L_\beta}$, $(I_{coh} + I_{Comp})/(\mu/\rho)_{K_{\alpha_2}}$, $(I_{coh} + I_{Comp})/(\mu/\rho)_{K_{\alpha_1}}$, $I_{L_\alpha}/I_{sc_{(L_\alpha)}}$, $I_{L_\beta}/I_{sc_{(L_\beta)}}$, $I_{K_{\alpha_2}}/I_{sc_{(K_{\alpha_2})}}$ and $I_{K_{\alpha_1}}/I_{sc_{(K_{\alpha_1})}}$ intensity ratios were also calculated.

2. Experimental

The schematic of the experimental set-up to be used in this study is shown in Figure 1. The samples were placed in the sample holder located in a chamber called the sample chamber. Thanks to the sample room where the samples were placed, the effects from the air environment were reduced and the best spectrum was tried to be obtained. The 5 Curie (Ci) Americium-241 (Am^{241}) annular source in the sample room was placed in a conical lead collimator. Lead shielding in the sample room was made to prevent harm to the researcher during measurements.

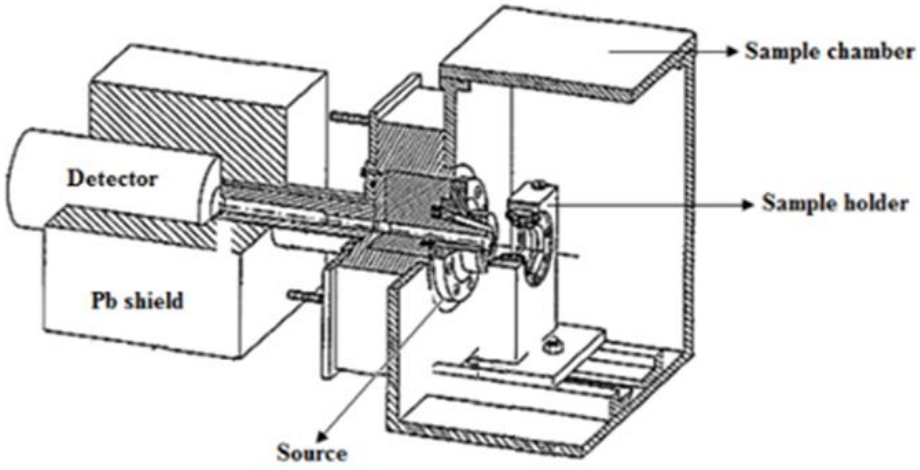

Figure 1. Experimental set up for determination different intensity ratios of samples with atomic numbers. The detector is HPGe detector and the source is Am-241.

An HpGe detector was used to count x-rays. Information about the detector used in this study can be found in Table1.The counting time for each sample is 3600 seconds. In this study, fourteen different samples were prepared using the dilution technique. Samples with different mean atomic numbers were obtained by mixing bismuth (Bi) and cellulose ($C_6H_{10}O_5$) powders. Mean atomic number of cellulose is given by

$$\bar{Z}_c = \frac{\sum_i n_i Z_i}{n} \quad (1)$$

where n is total number of atoms in cellulose, n_i is the number of atoms of the element i., and Z_i is the atomic number of the element i.

Table 1. Some specific features of the detector used in this study.

Configuration	Planar
Resolution at 5.9 keV	182 eV
Crystal diameter	16 mm
Crystal length	10 mm
Beryllium window	0.12 mm
Active area	200 mm^2

The concentrations of bismuth and cellulose in the targets of cellulose are calculated by

$$C_{b(c)}\% = \frac{m_{b(c)}}{m_b + m_c} \times 100 \quad (2)$$

where m_b is the mass of the bismuth and m_c is the mass of the cellulose. The mean atomic number of the prepared samples is calculated by

$$\bar{Z}_s = \bar{Z}_b \times C_b + \bar{Z}_c \times C_c \quad (3)$$

where $\bar{Z}_s$ mean atomic number of the sample, $\bar{Z}_b$ and $\bar{Z}_c$ are the mean atomic numbers of bismuth and cellulose, respectively. Information about the samples used in this study can be found in Table 2.

The total scattering intensity at a given wavelength is expressed as follows [40]

$$I_{sc} = \frac{I_{coh}}{2(\mu/\rho)_{\lambda}} + \frac{I_{Comp}}{2(\mu/\rho)_{\lambda}+(\mu/\rho)_{\lambda-\Delta\lambda}} \quad (4)$$

where I_{coh} and I_{Comp} in equation show the areas under the coherent and Compton peak. $(\mu/\rho)_{\lambda}$mass absorption coefficient of the sample at a specific wavelength (at $K_{\alpha}, K_{\beta}, L_{\alpha}$, L_{β}) and $(\mu/\rho)_{\lambda-\Delta\lambda}$ is the mass absorption coefficient of the sample at the excitation photon energy.

Table 2. Masses, percentage ratios and average atomic numbers of the samples used in this study.

Sample No	m_b (g)	m_c (g)	C_b (%)	C_c (%)	Sample thickness (g/cm^2)	$\overline{Z}_s$
1	0.357	0.000	1.000	0.000	0.255	83.000
2	0.326	0.025	0.929	0.071	0.227	77.371
3	0.300	0.050	0.857	0.143	0.243	71.703
4	0.276	0.075	0.786	0.214	0.230	66.082
5	0.251	0.101	0.713	0.287	0.233	60.377
6	0.225	0.125	0.643	0.357	0.230	54.796
7	0.200	0.151	0.571	0.429	0.224	49.143
8	0.175	0.175	0.500	0.500	0.214	43.551
9	0.150	0.201	0.428	0.572	0.211	37.855
10	0.125	0.225	0.357	0.643	0.195	32.273
11	0.101	0.250	0.287	0.713	0.193	26.718
12	0.075	0.275	0.215	0.785	0.228	21.044
13	0.051	0.301	0.144	0.856	0.204	15.444
14	0.025	0.325	0.072	0.928	0.214	9.743

In addition $(I_{coh} + I_{Comp})/(\mu/\rho)_{L_\alpha}$, $(I_{coh} + I_{Comp})/(\mu/\rho)_{L_\beta}$, $(I_{coh} + I_{Comp})/(\mu/\rho)_{K_{\alpha_2}}$, $(I_{coh} + I_{Comp})/(\mu/\rho)_{K_{\alpha_1}}$, $I_{L_\alpha}/I_{sc_{(L_\alpha)}}$, $I_{L_\beta}/I_{sc_{(L_\beta)}}$, $I_{K_{\alpha_2}}/I_{sc_{(K_{\alpha_2})}}$ ve $I_{K_{\alpha_1}}/I_{sc_{(K_{\alpha_1})}}$ intensity ratios were calculated in this study. The theoretical mass attenuation coefficients were used from the study of Gerward et al. [41].

3. Results and Discussion

The typical spectra of emission (L_α and L_β) , Compton and coherent scattering peaks for samples of some mean atomic numbers are shown in the Fig. 2-4 respectively. When the given spectra are analyzed, the intensities of the characteristic peaks (Lα and Lβ) in Figure 2 and the coherent scattering peaks shown in Figure 4 increase with increasing mean atomic number. Since Compton scattering is dominant in samples with low atomic number, it can be seen in Figure 3 that the intensities of Compton scattering peaks decrease with increasing mean atomic number.

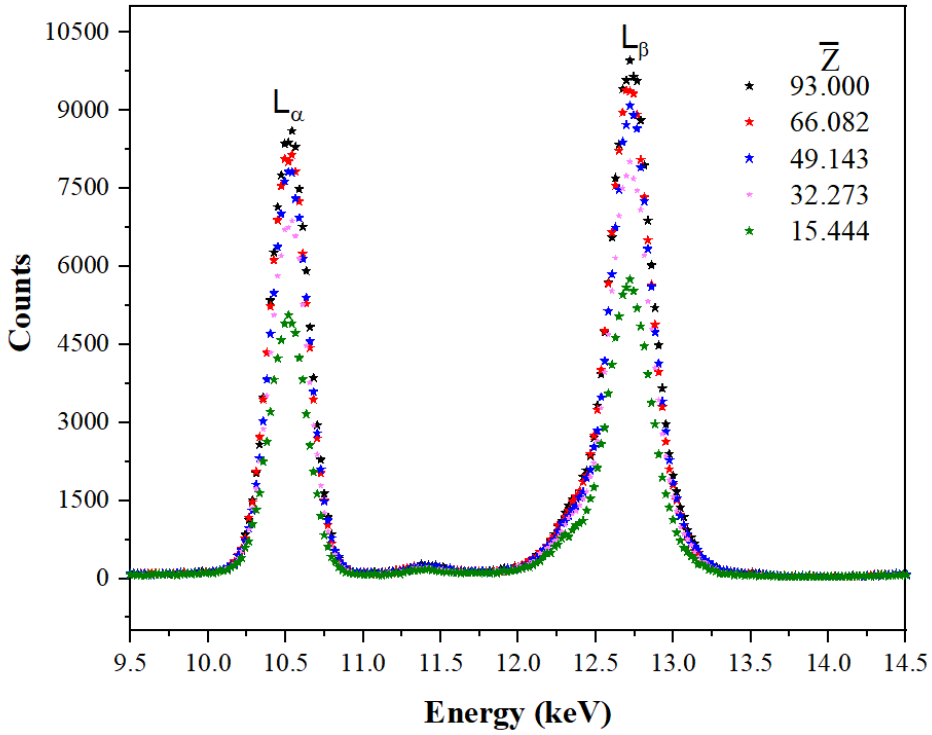

Figure 2. The typical energy dispersive Lα and Lβ characteristic x-ray peaks of some samples used in the study with atomic numbers between 9 and 83.

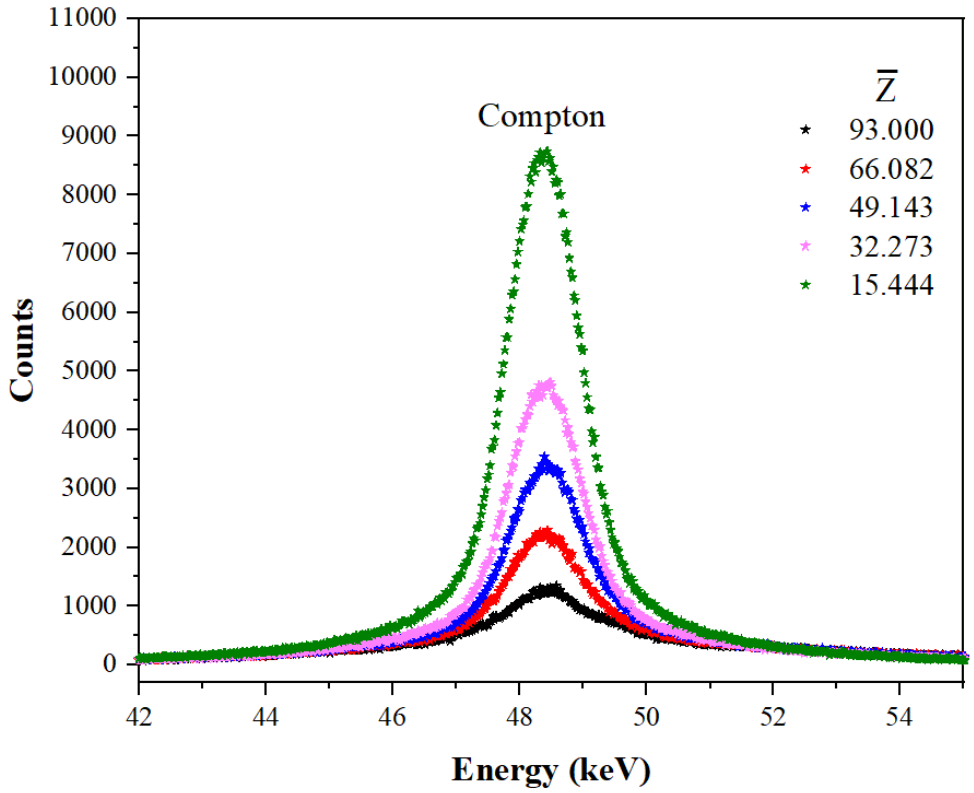

Figure 3. The typical Compton peaks of some samples used in the study with atomic numbers between 9 and 83.

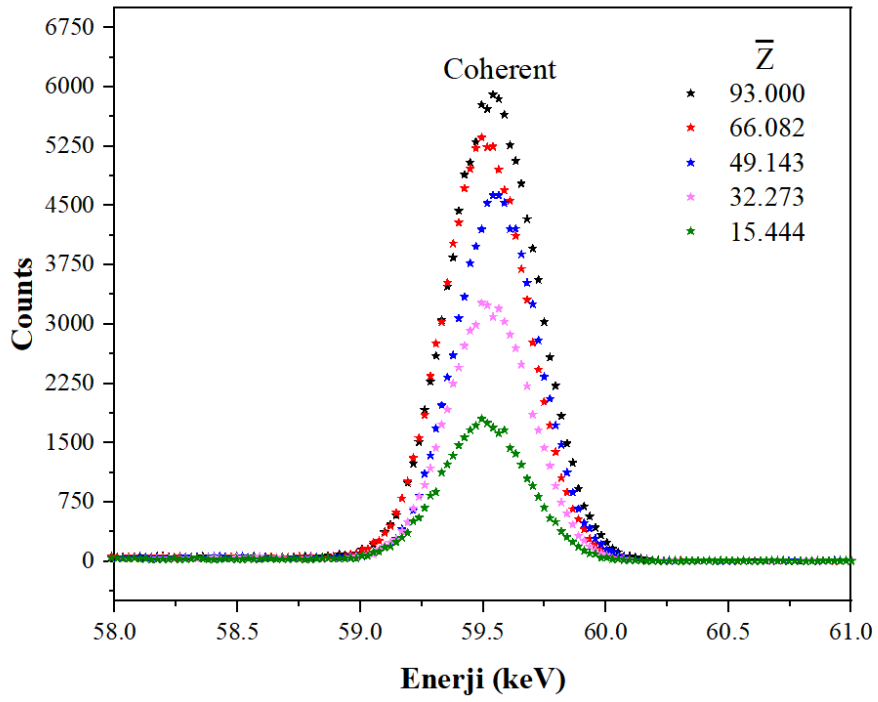

Figure 4. The typical coherent peaks of some samples used in the study with atomic numbers between 9 and 83.

In this study, different intensity ratios of fourteen different samples with average atomic numbers between 9.743 and 83.000 were calculated. The changes in intensity ratios caused by small changes in atomic number have been studied. The total scattering intensity ratios of the obtained samples were calculated at four different energies. These energies are $K_{\alpha_1}, K_{\alpha_2}, L_\alpha, L_\beta$ energies of the bismuth element. The variation of total scattering intensity ratios with mean atomic number is given in Figure 5-8.

In this study the $(\mathrm{I_{coh}} + \mathrm{I_{Comp}})/(\mu/\rho)_{L_\alpha}$, $(\mathrm{I_{coh}} + \mathrm{I_{Comp}})/(\mu/\rho)_{L_\beta}$, $(\mathrm{I_{coh}} + \mathrm{I_{Comp}})/(\mu/\rho)_{K_{\alpha_2}}$, $(\mathrm{I_{coh}} + \mathrm{I_{Comp}})/(\mu/\rho)_{K_{\alpha_1}}$ scattering ratios with mean atomic number is given Figure 9-12. Finally $I_{L_\alpha}/I_{sc_{(L_\alpha)}}$, $I_{L_\beta}/I_{sc_{(L_\beta)}}$, $I_{K_{\alpha_2}}/I_{sc_{(K_{\alpha_2})}}$ ve $I_{K_{\alpha_1}}/I_{sc_{(K_{\alpha_1})}}$ ratios are given Figure 13-16. Correlation coefficients were obtained for each scattering ratio with the Origin program. Correlation coefficient indicates the relationship between variables. The correlation coefficient approaching 1 indicates that the relationship between the variables is gradually increasing. As the correlation coefficient approaches 0, the relationship between the variables will gradually decrease.

As seen in Figure 5-8, the total scattering intensity ratios at $K_{\alpha_1}, K_{\alpha_2}, L_\alpha, L_\beta$ energies are fitted to exponential functions and their correlation coefficient is 0.999.As seen Figure 9-16 the correlation coefficients for $(\mathrm{I_{coh}} + \mathrm{I_{Comp}})/(\mu/\rho)_{L_\alpha}$, $(\mathrm{I_{coh}} + \mathrm{I_{Comp}})/(\mu/\rho)_{L_\beta}$, $(\mathrm{I_{coh}} + \mathrm{I_{Comp}})/(\mu/\rho)_{K_{\alpha_2}}$ and $(\mathrm{I_{coh}} + \mathrm{I_{Comp}})/(\mu/\rho)_{K_{\alpha_1}}$ are 0.972, 0.962, 0.980 and 0.982, respectively. Additionally, the correlation coefficients found for the intensity ratios $I_{L_\alpha}/I_{sc_{(L_\alpha)}}$, $I_{L_\beta}/I_{sc_{(L_\beta)}}$, $I_{K_{\alpha_2}}/I_{sc_{(K_{\alpha_2})}}$ ve $I_{K_{\alpha_1}}/I_{sc_{(K_{\alpha_1})}}$ are 0.988,0.994, 0.995 and 0.996.

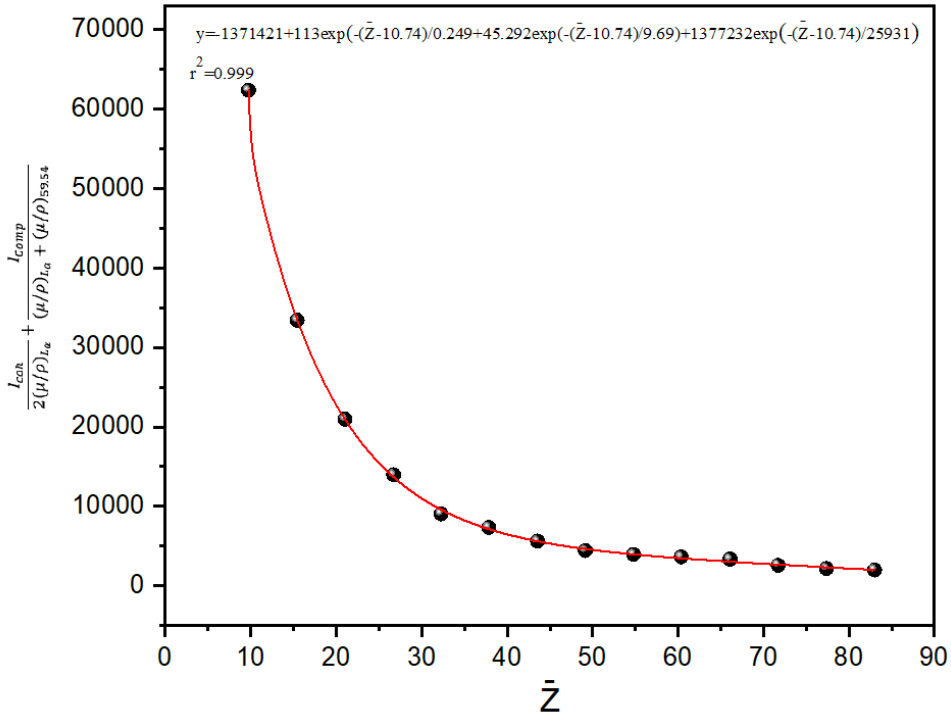

Figure 5. The variation of I_{sc} with mean atomic number at L_α energy.

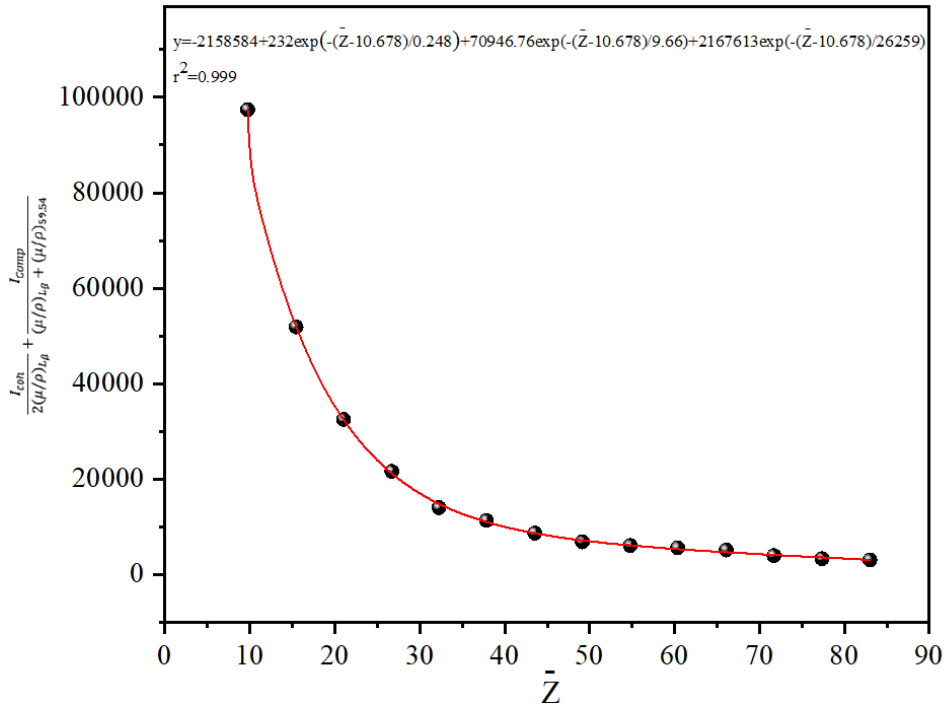

Figure 6. The variation of I_{sc} with mean atomic number at L_β energy

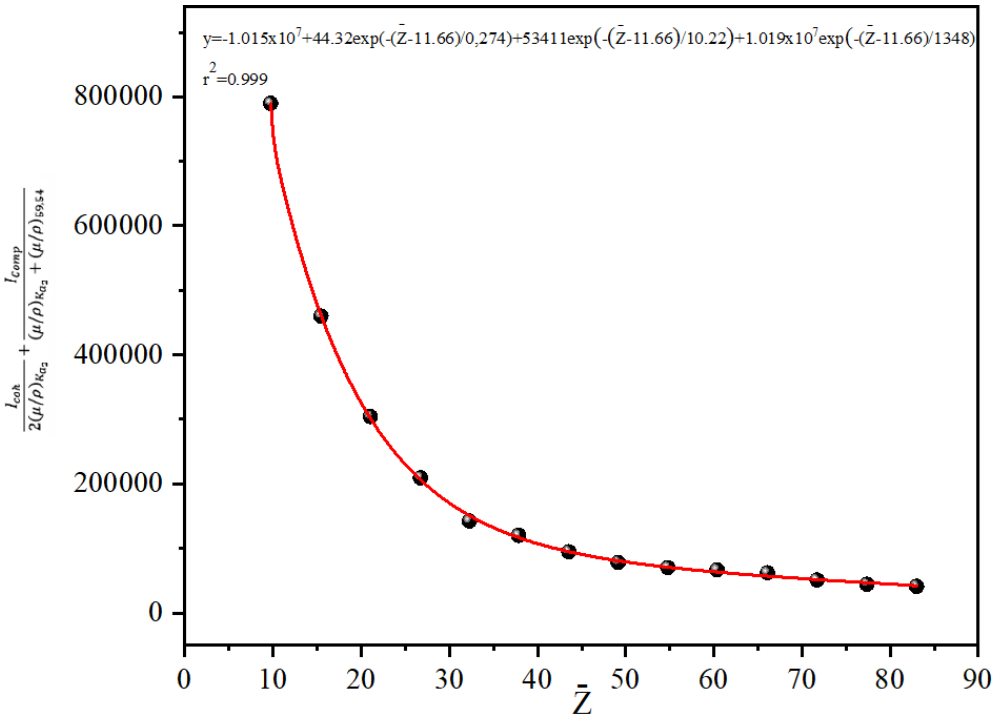

Figure 7. The variation of I_{sc} with mean atomic number at K_{α_2} energy.

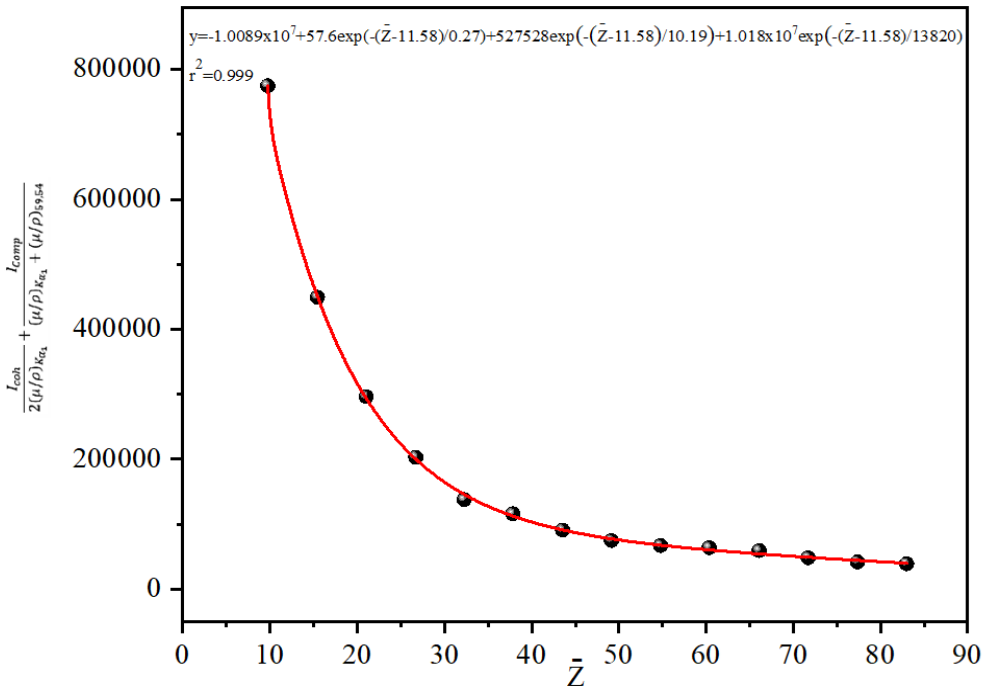

Figure 8. The variation of I_{sc} with mean atomic number at K_{α_1} energy.

In this study the $(\mathrm{I_{coh}} + \mathrm{I_{Comp}})/(\mu/\rho)_{L_\alpha}$, $(\mathrm{I_{coh}} + \mathrm{I_{Comp}})/(\mu/\rho)_{L_\beta}$, $(\mathrm{I_{coh}} + \mathrm{I_{Comp}})/(\mu/\rho)_{K_{\alpha_2}}$, $(\mathrm{I_{coh}} + \mathrm{I_{Comp}})/(\mu/\rho)_{K_{\alpha_1}}$ scattering ratios with mean atomic number is given Figure 9-12.

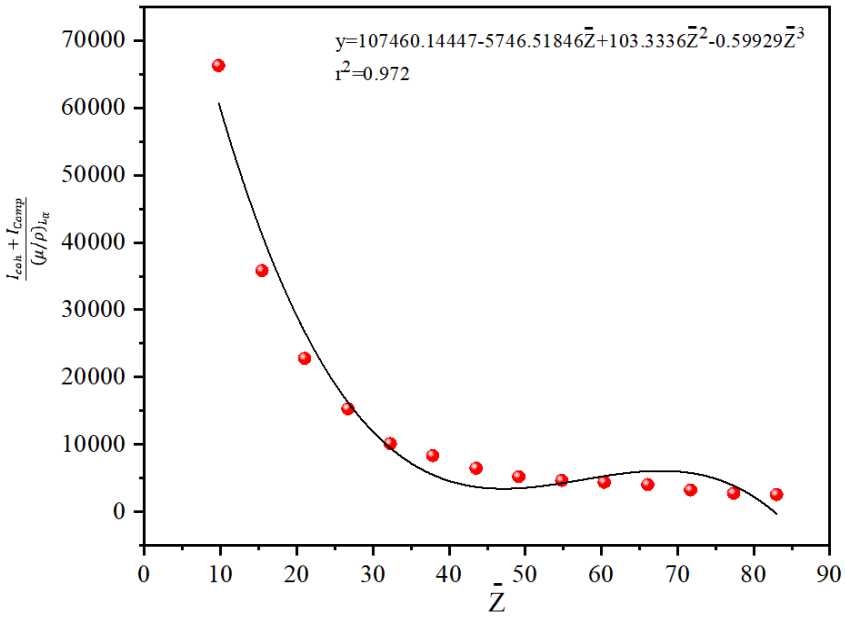

Figure 9. The variation of $I_{coh} + I_{Comp}/(\mu/\rho)_{L_\alpha}$ intensity ratios with mean atomic number. $\mathrm{I_{coh}}$ and $\mathrm{I_{Comp}}$ are elastic and inelastic scattering intensities and $(\mu/\rho)_{L_\alpha}$ shows the mass absorption coefficient at L_α energy.

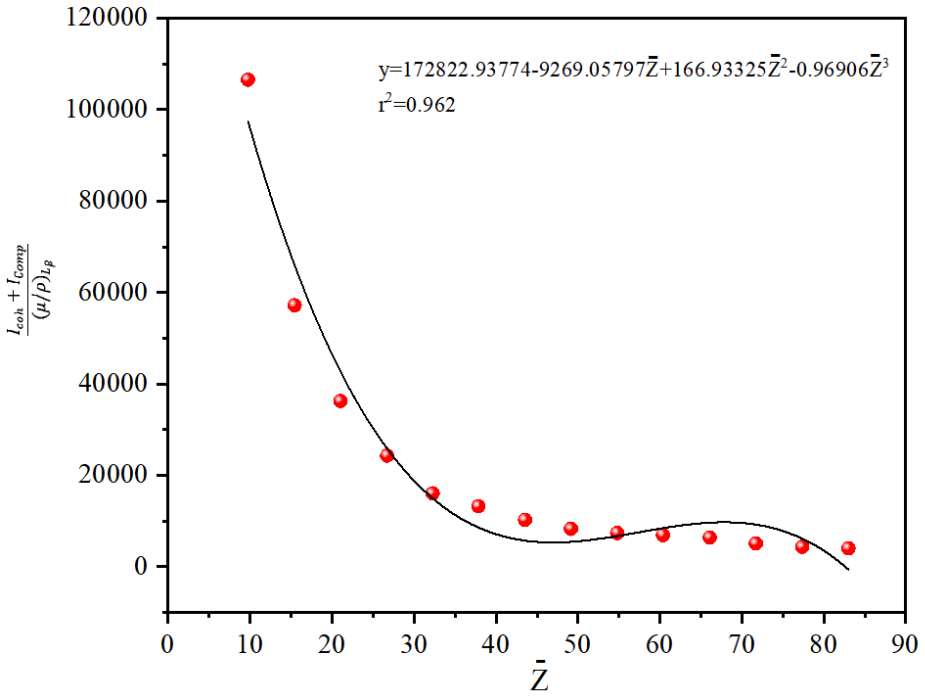

Figure 10. The variation of $I_{coh} + I_{Comp}/\ (\mu/\rho)_{L_\beta}$ intensity ratios with mean atomic number. I_{coh} and I_{Comp} are elastic and inelastic scattering intensities and $(\mu/\rho)_{L_\beta}$ shows the mass absorption coefficient at L_β energy.

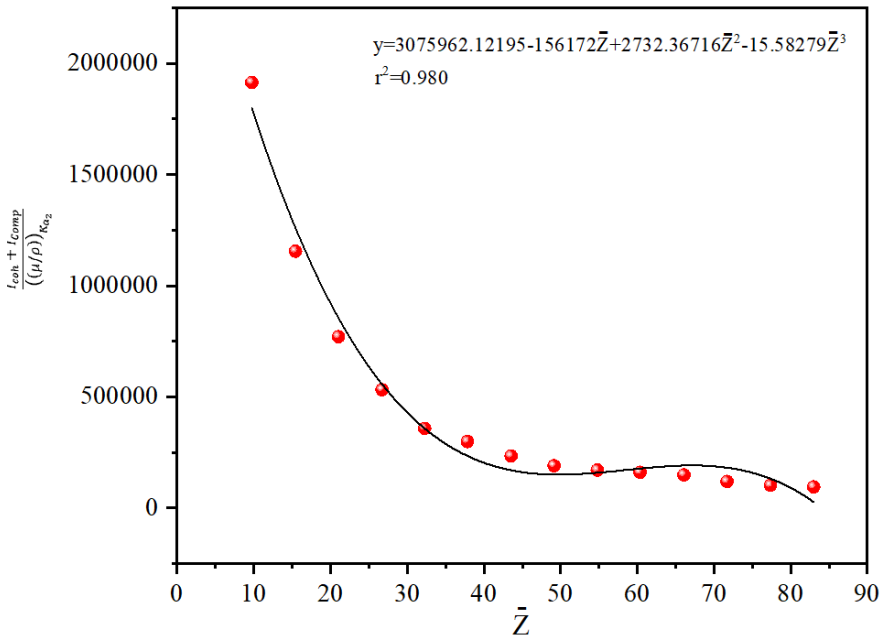

Figure 11. The variation of $I_{coh} + I_{Comp}/\ (\mu/\rho)_{K_{\alpha_2}}$ intensity ratios with mean atomic number. I_{coh} and I_{Comp} are elastic and inelastic scattering intensities and $(\mu/\rho)_{K_{\alpha_2}}$ shows the mass absorption coefficient at K_{α_2} energy.

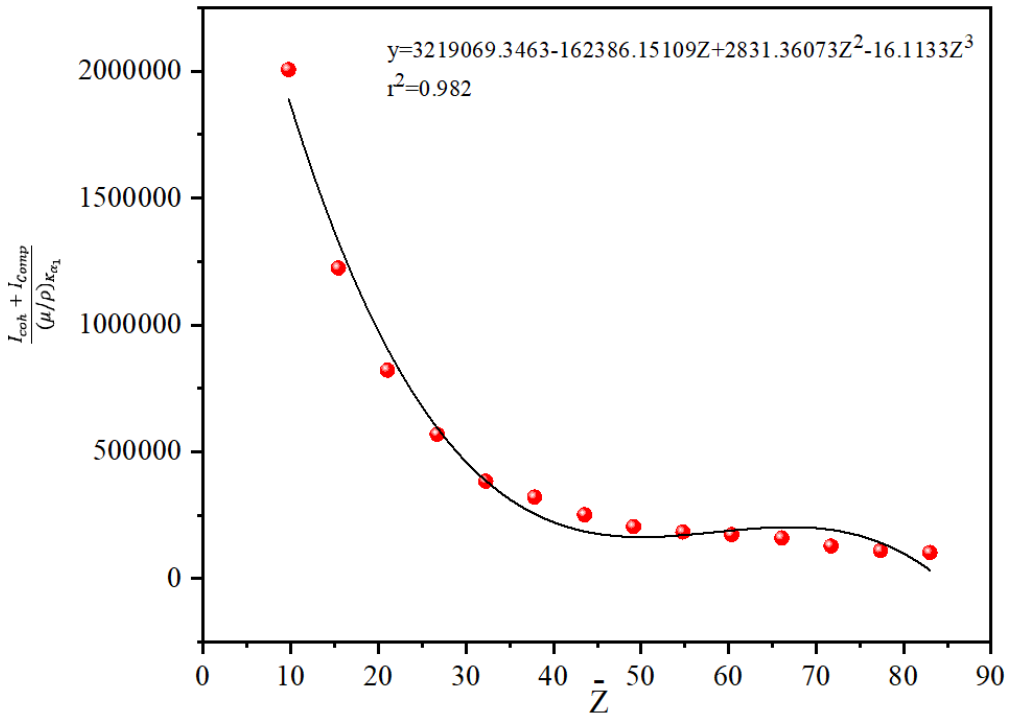

Figure 12. Variation of $I_{coh} + I_{Comp}/\ (\mu/\rho)_{K_{\alpha_1}}$ intensity ratios with mean atomic number. . I_{coh} and I_{Comp} are elastic and inelastic scattering intensities and $(\mu/\rho)_{K_{\alpha_1}}$ shows the mass absorption coefficient at K_{α_1} energy.

Finally $I_{L_\alpha}/I_{sc_{(L_\alpha)}}, I_{L_\beta}/I_{sc_{(L_\beta)}}$, $I_{K_{\alpha_2}}/I_{sc_{(K_{\alpha_2})}}$ ve $I_{K_{\alpha_1}}/I_{sc_{(K_{\alpha_1})}}$ ratios are given Figure 13-16. Correlation coefficients were obtained for each scattering ratio with the Origin program. Correlation coefficient is a coefficient that shows the relationship between variables. The correlation coefficient approaching 1 indicates that the relationship between the variables is gradually increasing. As the correlation coefficient approaches 0, the relationship between the variables will gradually decrease.

As seen in Figure 5-8, the total scattering intensity ratios at $K_{\alpha_1}, K_{\alpha_2}, L_\alpha, L_\beta$ energies are fitted to exponential functions and their correlation coefficient is 0.999.As seen Figure 9-16 the correlation coefficients for $(\mathrm{I_{coh}} + \mathrm{I_{Comp}})/\ (\mu\ /\ \rho)_{L_\alpha}$, $(\mathrm{I_{coh}} + \mathrm{I_{Comp}})/\ (\mu\ /\ \rho)_{L_\beta}$, $(\mathrm{I_{coh}} + \mathrm{I_{Comp}})/\ (\mu\ /\ \rho)_{K_{\alpha_2}}$ and $(\mathrm{I_{coh}} + \mathrm{I_{Comp}})/\ (\mu\ /\ \rho)_{K_{\alpha_1}}$ are 0.972, 0.962, 0.980 and 0.982, respectively. Additionally, the correlation coefficients found for the intensity ratios $I_{L_\alpha}/I_{sc_{(L_\alpha)}}, I_{L_\beta}/I_{sc_{(L_\beta)}}, I_{K_{\alpha_2}}/I_{sc_{(K_{\alpha_2})}}$ ve $I_{K_{\alpha_1}}/I_{sc_{(K_{\alpha_1})}}$ are 0.988,0.994, 0.995 and 0.996.

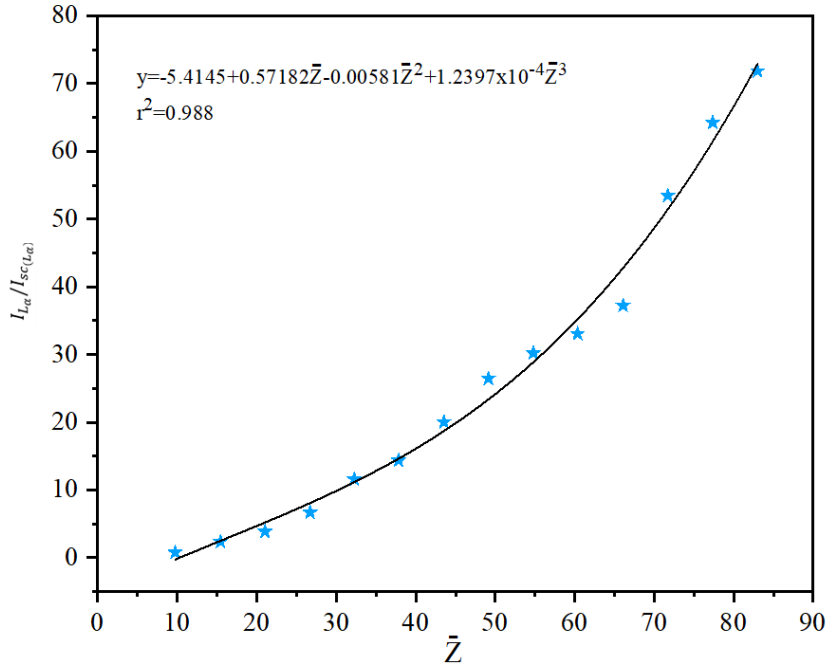

Figure 13. The variation of $I_{L_\alpha}/I_{sc_{(L_\alpha)}}$ intensity ratios with mean atomic number. I_{L_α} is intensity under the L_α peak and $I_{sc_{(L_\alpha)}}$ is the total scattering intensity at L_α energy.

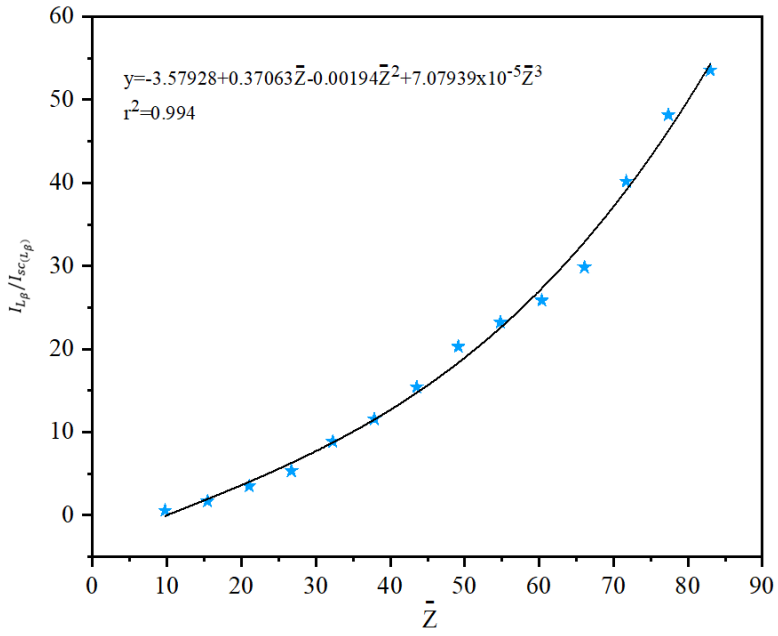

Figure 14. The variation of $I_{L_\beta}/I_{sc_{(L_\beta)}}$ intensity ratios with mean atomic number. I_{L_β} is intensity under the L_β peak and $I_{sc_{(L_\beta)}}$ is the total scattering intensity at L_β energy.

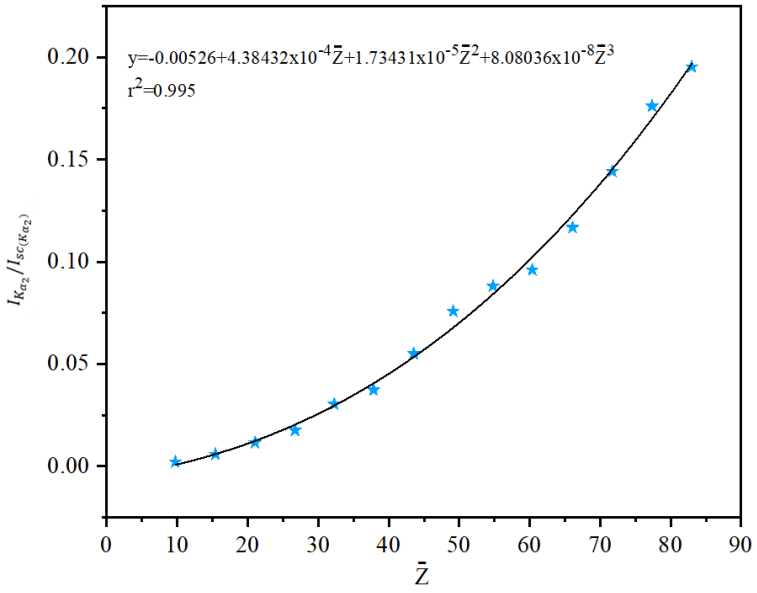

Figure 15. The variation of $I_{K_{\alpha_2}}/I_{sc_{(K_{\alpha_2})}}$ intensity ratios with mean atomic number. $I_{K_{\alpha_2}}$ is intensity under the $I_{K_{\alpha_2}}$ peak and $I_{sc_{(K_{\alpha_2})}}$ is the total scattering intensity at K_{α_2} energy.

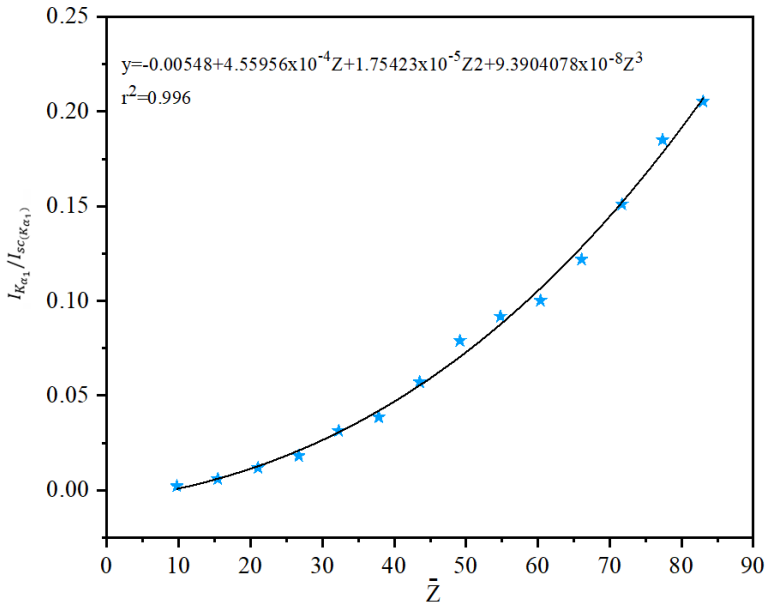

Figure 16. The variation of $I_{K_{\alpha_1}}/I_{sc_{(K_{\alpha_1})}}$ intensity ratios with mean atomic number. $I_{K_{\alpha_1}}$ is intensity under the $I_{K_{\alpha_1}}$ peak and $I_{sc_{(K_{\alpha_1})}}$ is the total scattering intensity at K_{α_1} energy.

4. Conclusions

In this study, different intensity ratios of fourteen samples with atomic numbers between 9.74 and 83.00 were calculated using the dilution technique. The changes of different intensity ratios with the mean atomic number are shown in graphs and correlation coefficients are calculated. As seen from Figure5-16 correlation coefficients are greater than 0.960. When the results are examined carefully, it shows that different intensity ratios can be used safely in the analysis of complex materials. It is also clear that qualitative analysis of complex materials can be performed using the dilution technique without the need for expensive standard samples.

Correlation coefficients provide information about the best intensity ratios that can be used to find the effective/equivalent atomic number of a complex material. As can be seen from the obtained fit curves, $I_{L_\alpha}/I_{sc_{(L_\alpha)}}$, $I_{L_\beta}/I_{sc_{(L_\beta)}}$ $I_{K_{\alpha_2}}/I_{sc_{(K_{\alpha_2})}}$ and $I_{K_{\alpha_1}}/I_{sc_{(K_{\alpha_1})}}$ intensity ratios are the best spectral ratio methods that can be used to determine the effective atomic number. Such studies will also help develop databases such as WinXCom and ANSI, which are used to find the effective atomic number theoretically and semiempirically.

Ethics in Publishing

There are no ethical issues regarding the publication of this study.

Author Contributions

Tuba AKKUŞ: Conceptualization, Methodology, Data, curation, Writing – original draft preparation.

Mehmet Fatih TEMİZ: Collecting data, evaluating the results, writing article.

References

[1] Hassib, Sonia T. Qualitative and quantitative analysis of uracil anticancer drugs. *Talanta* **1981**, 28(9), 685-687.

[2]Greil, J. D;Joly, B; Chanal, M; Cluzel, R. Qualitative and quantitative analysis of skin flora on hands after" hygienic type handwashing with a liquid soap and with a detergent bactericidal solution. Pathologie Biologie **1984**, 32(5).

[3]Svoboda, K. P; Hay, R. K; Waterman, P. G. Growing summer savory (Satureja hortensis) in Scotland: Quantitative and qualitative analysis of the volatile oil and factors influencing oil production. Journal of the Science of Food and Agriculture **1990**, 53(2), 193-202.

[4]Ekinci, N; Astam, N; Sahin, Y. Qualitative and quantitative analysis of the cataract using EDXRF. Journal of Quantitative Spectroscopy and Radiative Transfer, 2002, 72(6), 783-787.

[5]Jelesijevic, T; Jovanović, M; Knežević, M; Aleksić-Kovačević, S. Quantitative and qualitative analysis of Ag-NOR in benign and malignant canine mammary gland tumors, Acta Veterinaria-Beograd 2003, 53(5-6), 353-360.

[6]Ekinci, N; Gürol, A; Polat, R; Budak, G; Karabulut, A. The qualitative and quantitative analysis of Sarıkamış ore by energy dispersive X-ray fluorescence. Journal of Radioanalytical and Nuclear Chemistry **2003**, 258 (1), 163-165.

[7] Linati, L; Lusvardi, G; Malavasi, G; Menabue, L; Menziani, M. C; Mustarelli, P; Segre, U. Qualitative and Quantitative Structure− Property Relationships Analysis of Multicomponent Potential Bioglasses. The Journal of Physical Chemistry B **2005**, 109(11), 4989-4998.

[8]Huerta, V. D; Sánchez, M. L. F; Sanz-Medel, A. Qualitative and quantitative speciation analysis of water soluble selenium in three edible wild mushrooms species by liquid chromatography using post-column isotope dilution ICP–MS. Analytica Chimica Acta **2005**, 538(1-2), 99-105.

[9]Gunasekaran, S; Devi, T. R; Sakthivel, P. S. Qualitative and quantitative analysis on fibrates-A spectroscopic study. Asian Journal of Chemistry 2008, 20(6), 4249.

[10]Oilo, M; Tvinnereim, H. M; Gjerdet, N. R. Qualitative and quantitative fracture analyses of high-strength ceramics. European Journal of Oral Sciences **2009**,117(2), 187-193.

[11] Ge, J; Liu, Z; Zhi, Z; Zhao, X. S. Qualitative and quantitative thrombin analysis in serum using aptamers and gold nanoparticles through progressive dilution. Analytical Biochemistry **2011**, 413(1), 75-77.

[12] Qin, Y; Liu, J; Wang, G; Zhang, Y. Evaluation of indoor air quality based on qualitative, quantitative and olfactory analysis. Chinese Science Bulletin, 2013,58(9), 986-991.

[13]Vesnin, V. L. Qualitative Analysis of Liquid Hydrocarbon Mixtures by Absorption Spectra of Their Vapors. Journal of Applied Spectroscopy 2016, 83(5), 840-844.

[14]Brenz, F; Linke, S; Simat, T. (2017). Qualitative and quantitative analysis of monomers in polyesters for food contact materials. Food Additives & Contaminants: Part A **2017** 34(2), 307-319.

[15]Tzima, K; Brunton, N. P; Rai, D. K. Qualitative and quantitative analysis of polyphenols in Lamiaceae plants-A review. Plants **2018**, 7(2), 25.

[16]Tang, Y;Si, G; Sun, W; Li, B; Li, D; Hu, X. Analysis of temperature adaptability of qualitative analysis model for liquid multicomponent mixtures. Optik **2019**,198, 163221.

[17]Obata, Y; Bale, H. A; Barnard, H. S; Parkinson, D. Y; Alliston, T; Acevedo, C. Quantitative and qualitative bone imaging: A review of synchrotron radiation microtomography analysis in bone research. Journal of the mechanical behavior of biomedical materials 2010, 110, 103887.

[18]Faniran, T. S; Nkamba, L. N; Manga, T. T. Qualitative and Quantitative Analyses of COVID-19 Dynamics Axioms **2021**, 10(3), 210.

[19]Pedro, S. A; Rwezaura, H; Mandipezar, A; Tchuenche, J. M. Qualitative Analysis of an influenza model with biomedical interventions. Chaos, Solitons & Fractals **2019**, 146, 110852.

[20] Chechko, V. E. Qualitative analysis of the clustering in water solutions of alcohols III. Ukrayins' kij Fyizichnij Zhurnal (Kyiv) 2021, 66(10), 865-872.

[21] Fancher, C. M. Diffraction Methods for Qualitative and Quantitative Texture Analysis of Ferroelectric Ceramics Materials **2021**, 14(19), 5633.

[22]Koscielniak, P. Calibration methods in qualitative analysis. TrAC Trends in Analytical Chemistry **2022**, 150, 116587.

[23]Mititelu, M; Neacșu, S. M; Oprea, ; Dumitrescu, D. E;Nedelescu, M;Drăgănescu, D; Ghica, M. Black Sea Mussels Qualitative and Quantitative Chemical Analysis: Nutritional Benefits and Possible Risks through Consumption. Nutrients **2022**, 14(5), 964.

[24]Ott, J;Burghardt, A; Britz, D; Majauskaite, S; Mücklich, F. Qualitative and Quantitative Microstructural Analysis of Copper for Sintering Process Optimization in Additive Manufacturing Application. Practical Metallography **2021**, 58(1), 32-47.

[25] Doomen, R. A; Nedeljkovic, I; Kuitert, R. B; Kleverlaan, C. J;Aydin, B. Corrosion of orthodontic brackets: qualitative and quantitative surface analysis. The Angle Orthodontist **2022**, 92(5),661-668.

[26]He, S. H; Jiang, H. Qualitative and quantitative analysis of some co-existing colorants in some hard candies. Journal of Food Composition and Analysis **2022**, 109, 104475.

[27]Porikli, S.Chemical shift and intensity ratio values of dyspersium, holmium and erbium L X-ray emission lines . Radiation Physics and Chemistry **2012**,81(2),113-117.

[28]Yılmaz, R. Kb/Ka X-ray intensity ratios for some elements in the atomic number range 28≤Z≤39 at 16.896 keV Journal of Radiation Research and Applied Sciences **2017**, 10, 172-177.

[29] Sakar, E;Gurol, A; Bastug A. Experimental K X-ray intensity ratios of some heavy elements. Radiation Physics and Chemistry **2017**,131, 105-107.

[30]Yılmaz, R. Kβ/Kα X-Ray Intensity Ratios for Cr, Mn, Fe, and Co Excited by 8.735 keV Energy. Acta Physıca Polonıca A **2018**, 133, 5.

[31]Ugurlu, M.; Alım,B; Demir,L. The relationship between the external magnetic field and K X-ray intensity ratios of immiscible MoxAg1-x alloys, Radiation Physics and Chemistry **2019**, 165, 108396.

[32] Cengiz, E; Köksal, O; Apaydın, G; Karahan, İ; Ünal, E. Determination of valence electronic structure of Ni in Ni-B alloy coatings using Kβ-to-Kα X-ray intensity ratios. Applied Radiation and Isotopes, **2019**, 144, 24-28.

[33]Ugurlu, M; Demir,L. Relative K X-ray intensity ratios of the first and second transition elements in the magnetic field. Journal of Molecular Structure **2020**,1203, 127458

[34]Ismail, A. M; Malhi, N. B. L-shell x-ray relative intensities of some heavy elements excited by 20.48 keV x-rays. X-Ray Spectrometry **2000**, 29(4), 317-319

[35]Tırasoglu, E; Çevik, U; Ertugral, B; Apaydın, G;Ertugrul, M; Kobya, A. I. Chemical effects on Lα, Lβ, Lγ, Ll, and Lη X-ray production cross-sections and Li/Lα X-ray intensity ratios of Hg, Pb and Bi compound at 59.54 keV. The European Physical Journal D **2003**,26, 231-236

[36] Turgut, U; Ertuğrul, M. L X-ray intensity ratios for elements in the range $74 \leq Z \leq 92$ at 31.635 keV", Nuclear Instruments and Methods in Physics Research Section B **2004**, 222(3-4), 432-436.

[37]Yalçın, P; Porikli S; Kurucu, Y; Şahin, Y. Measurement of relative L X-ray intensity ratio following radioactive decay and photoionization. Physics Latters B **2008**, 663,3, 186-190.

[38] Porikli, S; Demir, D; Kurucu, Y.Variation of Kβ/ Kα X-ray intensity ratio and lineshape with the effects of external magnetic field and chemical combination. European Physical Journal D **2008**, 47,3, 315-323.

[39] Cinan, E; Ertuğrul, M; Aygün, B; Sayyed, M. I; Kurucu, Y; Özdemir, Y. Determination of the effect of temperature on relative L X-ray intensity ratio of gadolinium, dysprosium and erbium. Radiation Physics and Chemistry **2021**. 183, 109389.

[40] Bertin, E.P. Principles and practice of X-ray spectrometric analysis, second ed. Plenum Press, New York, 1975.

[41]Gerward, L; Guilbert, N; Jensen, K. B; Levring, H. X-ray absorption in matter Reengineering XCOM. Radiation Physics and Chemistry 2001, 60, 23–24.